Commun. Comput. Phys.
doi: 10.4208/cicp.2014.m344

Vol. **17**, No. 5, pp. 1113-1126
May 2015

Lattice Boltzmann Simulations of Thermocapillary Motion of Droplets in Microfluidic Channels

Jonathan Li[1], Haihu Liu[1,2,*], Nikolaos Ioannou[1], Yonghao Zhang[1] and Jason M. Reese[3]

[1] *James Weir Fluids Laboratory, Department of Mechanical & Aerospace Engineering, University of Strathclyde, Glasgow, G1 1XJ, United Kingdom.*
[2] *School of Energy and Power Engineering, Xi'an Jiaotong University, 28 West Xianning Road, Xi'an 710049, China.*
[3] *School of Engineering, University of Edinburgh, Edinburgh, EH9 3JT, United Kingdom.*

Received 31 October 2013; Accepted (in revised version) 21 May 2014

Abstract. Our recently developed lattice Boltzmann model is used to simulate droplet dynamical behaviour governed by thermocapillary force in microchannels. One key research challenge for developing droplet-based microfluidic systems is control of droplet motion and its dynamic behaviour. We numerically demonstrate that the thermocapillary force can be exploited for microdroplet manipulations including synchronisation, sorting, and splitting. This work indicates that the lattice Boltzmann method provides a promising design simulation tool for developing complex droplet-based microfluidic devices.

AMS subject classifications: 76T99

Key words: Lattice Boltzmann method, thermocapillary force, droplet manipulation, microfluidics.

1 Introduction

Droplet-based microfluidics has recently emerged as a promising, versatile platform for biological and chemical processes due to its advantages such as cost and time savings, improved analysis sensitivities, efficiency and accuracy. Unlike continuous-flow-based microfluidics, droplet-based microfluidics that creates discrete volumes with the use of immiscible fluids, allows for independent control of each droplet, thereby generating

*Corresponding author. *Email addresses:* haihu.liu@mail.xjtu.edu.cn (H. Liu), jonathan.li@strath.ac.uk (J. Li), nikolaos.ioannou@strath.ac.uk (N. Ioannou), yonghao.zhang@strath.ac.uk (Y. Zhang), jason.reese@ed.ac.uk (J. M. Reese)

droplet microreactors that can be individually processed for transportation, mixing and analysis [1]. Since reagents and samples can be confined in the droplets, it eliminates the issues associated with Taylor dispersion and surface adsorption, which can cause sample dilution and cross-contamination [2]. Droplet microfluidics offers great potential for performing a large number of reactions without increasing system size or complexity [3]. In addition, several studies [4,5] demonstrated that droplet microfluidics has the ability to implement simple Boolean logic functions, a critical step towards the realisation of a microfluidic computer.

Exploiting the benefits of droplet-based microfluidics efficiently, thus facilitating a wide range of applications, requires manipulation of droplets with high precision and flexibility. The most commonly encountered droplet manipulations include droplet generation, fission, fusion, mixing and sorting. Diverse mechanisms have been used for these droplet manipulations, including hydrodynamic stress, electrowetting, magnetic force, optical forces, thermocapillary force, surface acoustic waves, and dielectrophoresis [6]. Among these, thermocapillary force becomes increasingly attractive because it can be generated easily by means of substrate embedded microheaters [7,8] or by laser heating [9,10], which allows contactless, reconfigurable, and real-time control of multiple droplets without the need for any special microfabrication or moving parts. To date, the thermocapillary force has been combined with the geometry of the microchannel to realise various droplet manipulations including mixing, sorting, fission, fusion, sampling and switching [11,12].

Experimental studies have helped to understand thermocapillary flows in microfluidic devices, but it is still very difficult to conduct precise experimental measurements of the local temperature and flow fields during the transport process of a droplet. Thus, current applications of microfluidics are very largely done by experimental trial and error. Numerical modelling and simulations can complement experimental studies, providing an efficient pathway to enhance our understanding of dynamical droplet behaviour at the microscale. However, it is challenging to use traditional CFD (computational fluid dynamics) methods, e.g., the volume-of-fluid (VOF) [13] and level-set (LS) [14] methods, for simulating thermocapillary flows in microchannels because of numerical instability arising at the interface region when the interfacial tension becomes a dominant factor in microdroplet behavior [15]. Also, minimising the spurious velocities at the interface still remains a major challenge for these methods. In addition, a suitable slip model with slip length at the molecular scale has to be introduced to avoid stress singularities at the moving contact-line. Microscopically, the interface between different phases and the contact-line dynamics on the solid surface are due to interparticle interactions [16]. Thus, mesoscopic level models are expected to describe accurately the thermocapillary flows in a microchannel.

Recently, the lattice Boltzmann method (LBM) has developed into a promising alternative to traditional CFD methods for simulating complex fluid flow problems. LBM is a pseudo molecular method based on particle distribution functions that performs microscopic operations with mesoscopic kinetic equations and reproduces macroscopic

behaviour. Its mesoscopic kinetic nature offers many of the advantages of molecular dynamics, making LBM particularly suited for modelling multiphase, multicomponent flows. A number of multiphase, multicomponent models have been proposed in the LBM community, which can be classified into four major types: colour-fluid model [18], phase-field-based model [19, 20], interparticle-potential model [21], and mean-field theory model [22]. These models have been applied successfully to simulate various multiphase flow problems with a constant interfacial tension [23]. In Ref. [24], Liu et al. proposed the first thermocapillary LBM based on the colour-fluid model, which used the concept of continuum surface force (CSF) to model the capillary and Marangoni forces, and a recolouring algorithm by Latva-Kokko and Rothman [25] to produce phase separation. Later, Liu et al. developed two phase-field-based thermocapillary models with one focusing on high-density-ratio two-phase flows [26] and the other on modelling fluid-wall interactions [27]. The phase-field-based model can effectively eliminate unphysical spurious velocities at the phase interface. Small droplets or bubbles in the phase-field-based model, however, are prone to dissolve, when the multiphase system evolves to minimise the free energy. In contrast, the colour-fluid model can ensure strict mass conservation of each fluid. Although the study by the thermocapillary colour-fluid model has demonstrated that thermocapillary forces induced by the laser heating can block the droplet motion [24], it is restricted to a relatively simple microfluidic channel with the absence of fluid-wall interactions, and the model's capability for droplet manipulations is not fully investigated. In this paper, we will use the thermocapillary colour model to study droplet dynamical behaviour in several different microchannels when the thermal gradients are introduced by substrate embedded microheaters. We will reveal that the thermocapillary actuation can be a promising route towards performing various microfluidic functions including synchronisation, sorting and splitting.

2 Lattice Boltzmann method

The lattice Boltzmann (LB) equation can be expressed as [17, 28, 29]

$$f_i(\boldsymbol{x}+\boldsymbol{e}_i\delta t,t+\delta t)-f_i(\boldsymbol{x},t)=\Omega_i(\boldsymbol{x},t), \tag{2.1}$$

where $f_i(\boldsymbol{x},t)$ and $\Omega_i(\boldsymbol{x},t)$ are the particle distribution function and collision operator in the ith direction at the position $\boldsymbol{x}$ and the time t; δt is the time step, $\boldsymbol{e}_i$ is the lattice velocity in the ith direction, which is defined as $\boldsymbol{e}_0=(0,0)$, $\boldsymbol{e}_{1,3}=(\pm c,0)$, $\boldsymbol{e}_{2,4}=(0,\pm c)$, $\boldsymbol{e}_{5,7}=(\pm c,\pm c)$, and $\boldsymbol{e}_{6,8}=(\mp c,\pm c)$ for the two-dimensional 9-velocity (D2Q9) model, where $c=\delta_x/\delta_t$ is the lattice speed and δ_x is the lattice spacing. The most commonly used collision operator is the single relaxation time Bhatnagar-Gross-Krook (BGK) collision operator [30, 31] which is given by

$$\Omega_i(\boldsymbol{x},t)=-\frac{1}{\tau_f}(f_i(\boldsymbol{x},t)-f_i^{eq}(\boldsymbol{x},t)), \tag{2.2}$$

where τ_f is the relaxation time, and f_i^{eq} is the equilibrium distribution function, which is defined as [32]

$$f_i^{eq}(\boldsymbol{x},t)=\rho(\boldsymbol{x},t)\omega_i\left[1+\frac{\boldsymbol{e}_i\cdot\boldsymbol{u}(\boldsymbol{x},t)}{c_s^2}+\frac{1}{2}\frac{(\boldsymbol{e}_i\cdot\boldsymbol{u}(\boldsymbol{x},t))^2}{c_s^4}-\frac{1}{2}\frac{\boldsymbol{u}^2(\boldsymbol{x},t)}{c_s^2}\right], \tag{2.3}$$

where ρ and $\boldsymbol{u}$ are the local density and velocity, $c_s=1/\sqrt{3}c$ is the lattice sound speed, and w_i is the weight factor with $w_0=4/9$, $w_{1-4}=1/9$ and $w_{5-8}=1/36$. The density and momentum at each lattice node can be calculated using

$$\rho(\boldsymbol{x},t)=\sum_i f_i(\boldsymbol{x},t), \tag{2.4}$$

$$\rho\boldsymbol{u}(\boldsymbol{x},t)=\sum_i f_i(\boldsymbol{x},t)\boldsymbol{e}_i, \tag{2.5}$$

and the viscosity of the fluid is related to the relaxation time τ_f by

$$\nu=\left(\tau_f-\frac{1}{2}\right)c_s^2\delta_t. \tag{2.6}$$

To simulate thermocapillary flows, we use the colour-fluid LB model developed by Liu et al. [24]. In this model, the concept of CSF [33] is used to model the interfacial tension force and Marangoni stress, and a convection-diffusion equation is solved using the passive scalar approach to obtain the temperature field, which is coupled to the interfacial tension through an equation of state. The colour-fluid model introduces two particle distribution functions r_i and b_i to represent "red" and "blue" fluids. The total particle distribution function f_i is defined as

$$f_i(\boldsymbol{x},t)=r_i(\boldsymbol{x},t)+b_i(\boldsymbol{x},t), \tag{2.7}$$

which undergoes the collision and streaming operations as

$$f_i(\boldsymbol{x}+\boldsymbol{e}_i\delta t,t+\delta t)-f_i(\boldsymbol{x},t)=-\frac{1}{\tau_f}(f_i(\boldsymbol{x},t)-f_i^{eq}(\boldsymbol{x},t))+\Phi_i, \tag{2.8}$$

where Φ_i is the perturbation term, which contributes to the mixed interfacial regions and generates an interfacial force $\boldsymbol{F}$ [24,34]:

$$\Phi_i(\boldsymbol{x},t)=\left(1-\frac{1}{2\tau_f}\right)\omega_i\left[\frac{\boldsymbol{e}_i-\boldsymbol{u}(\boldsymbol{x},t)}{c_s^2}+\frac{\boldsymbol{e}_i\cdot\boldsymbol{u}(\boldsymbol{x},t)}{c_s^4}\boldsymbol{e}_i\right]\cdot\boldsymbol{F}(\boldsymbol{x},t)\delta t, \tag{2.9}$$

where $\boldsymbol{u}$ is the velocity of fluid mixture, which is redefined to incorporate the spatially varying interfacial force, i.e., [24,34,35]

$$\rho\boldsymbol{u}=\sum_i f_i\boldsymbol{e}_i+\frac{1}{2}\boldsymbol{F}\delta t. \tag{2.10}$$

Note that the equilibrium distribution function f_i^{eq} in Eq. (2.8) is still written in the form of Eq. (2.3), but the velocity in the equilibrium distribution function should use Eq. (2.10) instead of Eq. (2.5) due to the interfacial force involved.

An indicator function ρ^N is introduced to identify the location of interface, and is defined by

$$\rho^N(\boldsymbol{x},t)=\frac{\rho_r(\boldsymbol{x},t)-\rho_b(\boldsymbol{x},t)}{\rho_r(\boldsymbol{x},t)+\rho_b(\boldsymbol{x},t)}, \tag{2.11}$$

where ρ_r and ρ_b are the local densities of red and blue fluids and defined by

$$\rho_r(\boldsymbol{x},t)=\sum_i r_i(\boldsymbol{x},t), \tag{2.12}$$

$$\rho_b(\boldsymbol{x},t)=\sum_i b_i(\boldsymbol{x},t). \tag{2.13}$$

In the LBM community, the CSF concept [33] was first used by Lishchuk et al. [36] to model the interfacial force with a constant interfacial tension. It was later extended by Liu and Zhang [24] to model the interfacial force with a temperature-dependent interfacial tension and the Marangoni stress. Following [24], the interfacial force reads as

$$\boldsymbol{F}(\boldsymbol{x},t)=\frac{1}{2}|\nabla\rho^N|\nabla\cdot[\sigma(\boldsymbol{I}-\boldsymbol{n}\otimes\boldsymbol{n})]=\frac{1}{2}|\nabla\rho^N|(\sigma\kappa\boldsymbol{n}+\nabla_s\sigma), \tag{2.14}$$

where $\boldsymbol{I}$ is the second-order identity tensor, $\nabla_s=(\boldsymbol{I}-\boldsymbol{n}\otimes\boldsymbol{n})\cdot\nabla$ is the surface gradient operator, σ is the interfacial tension, $\boldsymbol{n}$ is the interfacial unit normal vector defined by

$$\boldsymbol{n}=\frac{\nabla\rho^N}{|\nabla\rho^N|}, \tag{2.15}$$

and κ is the local interface curvature related to $\boldsymbol{n}$ by

$$\kappa=-\nabla_s\cdot\boldsymbol{n}=-\nabla\cdot\boldsymbol{n}. \tag{2.16}$$

To account for temperature effects on the interfacial tension, the relationship

$$\sigma(T)=\sigma_{ref}+\sigma_T(T-T_{ref}) \tag{2.17}$$

is used, where T is the temperature, σ_{ref} is the interfacial tension at the reference temperature T_{ref}, and σ_T is the interfacial tension gradient with respect to temperature. In this study only a linear relationship between interfacial tension and temperature is used. Eq. (2.14) can then be modified to

$$\boldsymbol{F}(\boldsymbol{x},t)=\frac{1}{2}|\nabla\rho^N|[\sigma\kappa\boldsymbol{n}+\sigma_T(\boldsymbol{I}-\boldsymbol{n}\otimes\boldsymbol{n})\cdot\nabla T]. \tag{2.18}$$

To model the temperature field evolution, another particle distribution function g_i is used, with the governing equation

$$g_i(\boldsymbol{x}+\boldsymbol{e}_i\delta t,t+\delta t)-g_i(\boldsymbol{x},t)=-\frac{1}{\tau_g}(g_i(\boldsymbol{x},t)-g_i^{eq}(\boldsymbol{x},t)), \tag{2.19}$$

where τ_g is the relaxation parameter linked to the thermal diffusivity

$$k=\left(\tau_g-\frac{1}{2}\right)c_s^2\delta t, \tag{2.20}$$

and g_i^{eq} is the equilibrium distribution function

$$g_i^{eq}(\boldsymbol{x},t)=T(\boldsymbol{x},t)\omega_i\left[1+\frac{\boldsymbol{e}_i\cdot\boldsymbol{u}(\boldsymbol{x},t)}{c_s^2}+\frac{1}{2}\frac{(\boldsymbol{e}_i\cdot\boldsymbol{u}(\boldsymbol{x},t))^2}{c_s^4}-\frac{1}{2}\frac{\boldsymbol{u}^2(\boldsymbol{x},t)}{c_s^2}\right], \tag{2.21}$$

where the temperature T is calculated by $T=\sum_i g_i$. Using the Chapman-Enskog expansion, Eq. (2.19) can recover the following macroscopic equation when the velocity is given by Eq. (2.10), i.e.,

$$\partial_t T+\boldsymbol{u}\cdot\nabla T=\nabla\cdot(k\nabla T). \tag{2.22}$$

Note that thermal flows can also be modelled by the use of a multi-speed approach [46], which is regarded as an extension of the isothermal LBM. However, the multi-speed approach requires using a large set of discrete velocities along with higher-order velocity terms in the equilibrium distribution function, resulting in a higher computational cost than the currently used passive scalar approach. In addition, the multi-speed approach may suffer from severe numerical instability and an unphysical fixed Prandtl number.

The partial derivatives required for the curvature and normal vector calculations are obtained using the finite difference stencil. For example, for a variable h, its partial derivatives can be calculated by [37]

$$\partial_\alpha h(\boldsymbol{x},t)=\frac{1}{c_s^2}\sum_i \omega_i h(\boldsymbol{x}+\boldsymbol{e}_i\delta t,t)\boldsymbol{e}_{i\alpha}. \tag{2.23}$$

Although the perturbation term generates an interfacial tension and the Marangoni stress, it does not guarantee the immiscibility of both fluids. To promote phase segregation and maintain the interface, we use the recolouring algorithm proposed by Latva-Kokko and Rothman [25], which can effectively reduce the unphysical spurious velocities at the interface and overcome the lattice pinning problem [38, 39]. Following their algorithm, the post-collision, recoloured red and blue fluid particle distribution functions are

$$r_i=\frac{\rho_r}{\rho}f_i^*+\beta\frac{\rho_r\rho_b}{\rho}\omega_i\boldsymbol{e}_i.\boldsymbol{n}, \tag{2.24}$$

$$b_i=\frac{\rho_b}{\rho}f_i^*-\beta\frac{\rho_r\rho_b}{\rho}\omega_i\boldsymbol{e}_i.\boldsymbol{n}, \tag{2.25}$$

where f_i^* is the total distribution function after the collision operation, and β is a segregation parameter which is set to 0.7 for numerical stability and model accuracy [38, 39].

For the hydrodynamic boundary conditions, we impose a no-slip boundary condition at the microchannel walls by using the simple bounceback scheme halfway between the solid and fluid nodes [40], and specify a fixed velocity profile at the inlets of the microchannels and a fixed pressure boundary condition at the outlets of the microchannels following Zou and He [41]. For the thermal boundary conditions, the wall temperatures are specified by the method of Liu et al. [42].

3 Results and discussion

3.1 Droplet synchronisation using thermal gradients

In many microdroplet applications, the mixing of droplets containing different reagents is necessary. To ensure that droplets from different microchannel branches collide and merge, synchronisation mechanisms are necessary. Although microchannels have been designed to passively synchronise droplets [43], it may also be desirable to use active synchronisation strategies in many integrated lab-on-a-chip systems with multiple functions [44]. Here we numerically demonstrate the use of thermal gradients to synchronise droplets.

The simulation geometry is shown in Fig. 1 with two connected microchannels, where two droplets are initially placed at the inlets of these microchannels, with one droplet at each inlet. A thermal gradient is applied locally at the bottom microchannel, in the

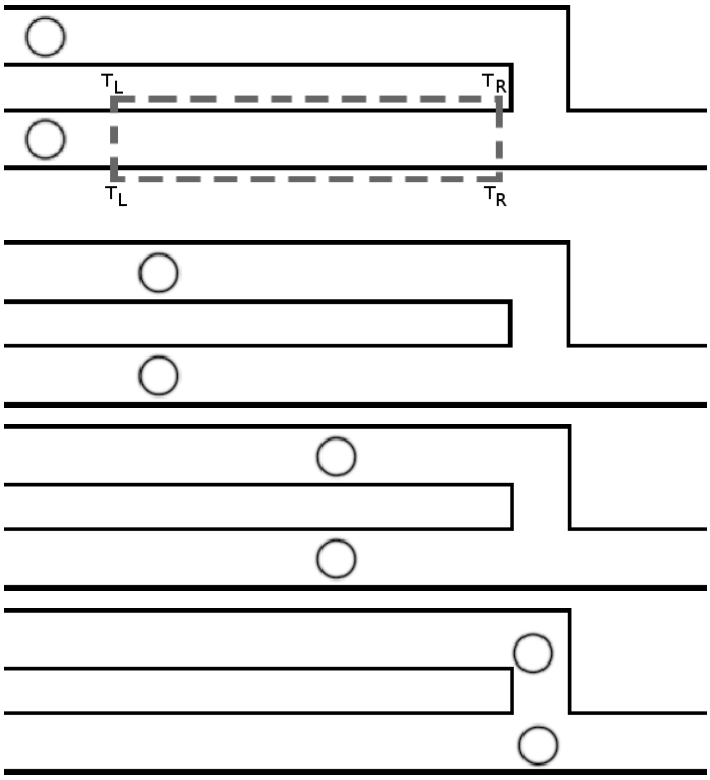

Figure 1: Simulation snapshots when no thermal gradient is applied at 0, 58000, 140000 and 206000 timesteps. The droplet in the lower microchannel reaches the channel intersection first as it has less distance to travel. For the non-isothermal cases, a linear thermal gradient is applied at the microchannel walls in the area within the dashed lines. The wall temperatures inside the dashed lines follow a linear distribution with the temperature T_L at the left hand side and T_R at the right hand side.

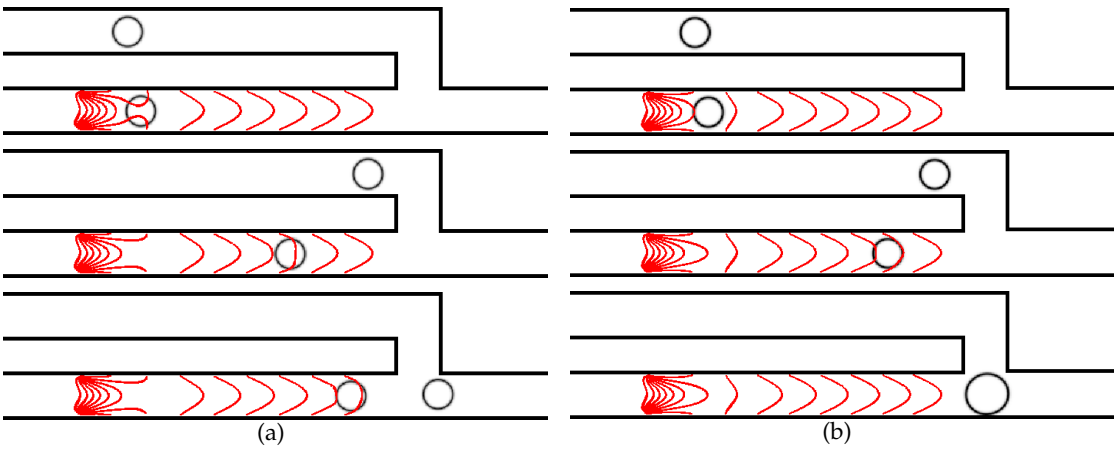

Figure 2: Evolution of droplet location and the temperature contours when a thermal gradient (indicated in red) is applied at the bottom microchannel with (a) $\sigma_T=-0.0015$ and (b) $\sigma_T=-0.001$ at 52000, 182000 and 244000 timesteps. In (a) the velocity of the droplet in the lower branch is significantly reduced while passing through the thermal gradient and as a result the droplet in the upper microchannel reaches the channel intersection first. Compared to (a), the droplet in (b) does not slow down as much due to a smaller σ_T, which leads to the droplets colliding and merging upon reaching the intersection.

area inside the dashed lines, by specifying the temperatures at the microchannel walls, where a high temperature T_L is specified at the left hand side which varies linearly to a temperature T_R at the right hand side. The fluid properties are chosen as $\rho_r=\rho_b=1$, $\nu_r=\nu_b=0.05$, $k_r=k_b=0.025$, $\sigma_{ref}=0.08$ and $T_{ref}=0$. The domain size of the simulation is 450×120 lattice units, and the droplets have a diameter of 30 lattice units. The average inlet channel velocity is fixed at u_{in}=0.003 for both channels. Note that all fluid properties are kept constant except the interfacial tension.

The simulation is first carried out under isothermal conditions, i.e. $T_L=T_R=0$. As shown in Fig. 1, both droplets travel at the same velocity, but the droplet in the lower microchannel will reach the intersection of both channels first as it has less distance to travel. Then a thermal gradient is applied on the bottom microchannel, where the temperature follows a linear distribution in the heated section with $T_L=30$ and $T_R=0$. Fig. 2(a) shows the evolution of droplet position and temperature field for $\sigma_T=-0.0015$. The droplet in the lower microchannel is observed to slow down while passing through the thermal gradient, which results in the droplet in the top microchannel reaching the channel intersection first. The droplet slows down because the thermal gradient in the lower microchannel causes a thermocapillary force to act opposite to the droplet's direction of travel. By changing the value of σ_T to -0.001, the droplet at the lower branch is slowed down just enough for the droplets in both branches to collide and merge as shown in Fig. 2(b). In both cases where a thermal gradient is applied the temperature profile is only slightly affected, which suggests that thermal gradients can provide thermocapillary force to synchronise multiple droplets.

3.2 Droplet sorting using thermal gradients

For biological and chemical analyses, samples are often required to be sorted for further processing and analysis. Since these sample droplets can have different σ_T, depending on the fluids used and the surfactants added, they can be exploited for sorting droplets under thermal gradients.

The microchannel geometry is shown in Fig. 3, where three microchannels are connected together. For each simulation a droplet is initially placed in the middle inlet microchannel and a thermal gradient is applied at the microchannel intersection, indicated by the area within the dashed lines in Fig. 3(a), where the top wall is at temperature $T_H = 20$ and the bottom wall is at temperature $T_L = 0$. The fluid properties are selected as $\rho_r = \rho_b = 1$, $\nu_r = \nu_b = 0.05$, $k_r = k_b = 0.025$, $\sigma_{ref} = 0.08$, $\sigma_T = -0.0001$ and $T_{ref} = 10$. The domain size of the simulation is 400×100 lattice units, and the droplets have a diameter of 20 lattice units. The velocity at each microchannel inlet is specified as u_{in}=0.003. Using these parameters, it is observed in Fig. 3(a) that the droplet migrates towards the top microchannel outlet, where the temperature is higher. At the microchannel intersection, the temperature difference between the top and bottom of the droplet creates an interfacial tension gradient, which causes a force to act upwards on the droplet.

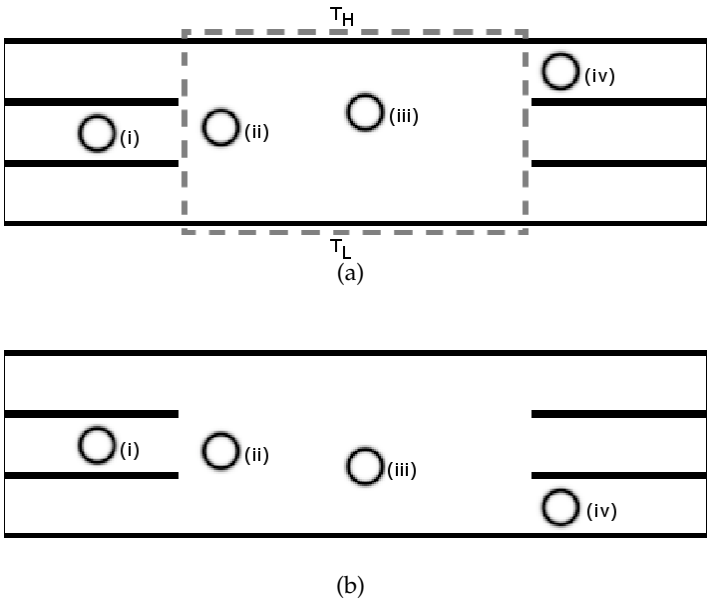

Figure 3: Droplet locations in sorting simulations for (a) $\sigma_T = -0.0001$ and (b) $\sigma_T = 0.0001$ at (i) 0, (ii) 40000, (iii) 84000 and (iv) 150000 timesteps. A thermal gradient is applied at the channel intersection, indicated by the area within the dashed lines in (a), by setting the temperature at the top wall to $T_H = 20$ and the temperature at the bottom wall to $T_L = 0$. In (a), as σ_T is negative, the thermal gradient at the channel intersection causes the droplet to move towards the top microchannel outlet. In (b), the droplet moves towards the bottom microchannel outlet as σ_T is positive.

By changing σ_T to 0.0001, the droplet is observed in Fig. 3(b) to migrate towards the lower microchannel branch, where the temperature of the fluid is lower. Since the interfacial tension dependency on the temperature gradient is positive, the thermocapillary force acts to move the droplet downwards, causing the droplet to exit through the bottom microchannel outlet. The results shown in Fig. 3 show that droplets with different σ_T can be sorted into different microchannels by use of thermal gradients. This demonstrates a new separation method for sorting droplets using thermal gradients.

3.3 Droplet splitting at a T-junction bifurcation

For the final simulation case the microchannel geometry in Fig. 5 is used, where the microchannel splits into two and the lower microchannel branch is heated near the inlet in the area specified within the dashed lines. Here we study the effects of thermocapillarity on droplet splitting and compare our simulation results to those obtained in a previously published experiment by Yap et al. [45], in which a microheater is embedded on one side of the microchannel near the inlet of the lower microchannel branch. The simulation domain size is 1000×1000 lattice units and the simulation parameters are set to be $\rho_r=\rho_b=1$, $\nu_r=\nu_b=0.05$, $k_r=k_b=0.025$, $\sigma_{ref}=0.05$, $\sigma_T=-0.002$ and $T_{ref}=0$. The main channel and the branch channels have a width of 100 and 50 lattices, respectively. The droplet plug is initially placed in the main channel with a length of 168 lattices. The mean velocity at the inlet is given as $u_{in}=0.025$.

When the heater is not turned on and the droplet reaches the intersection, the vis-

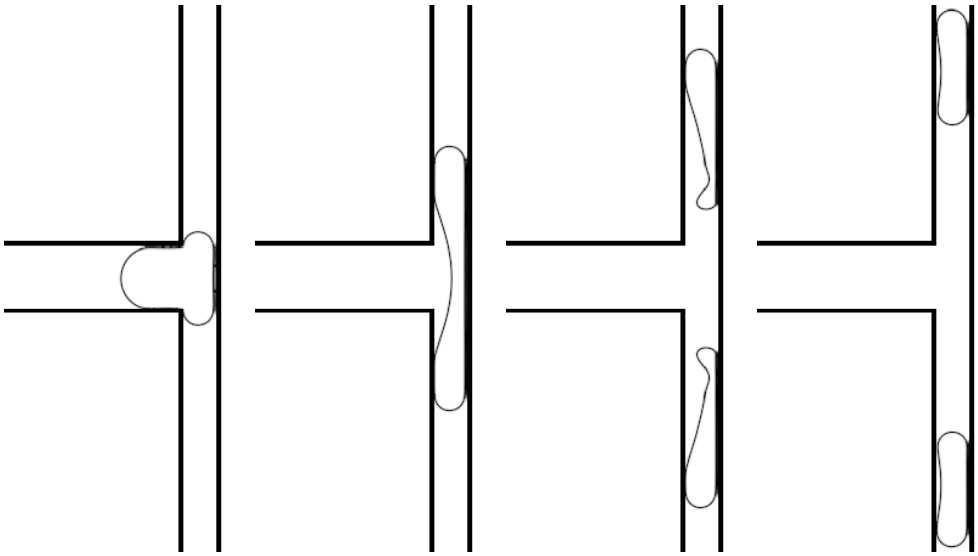

Figure 4: Droplet splitting at the T-junction under isothermal condition at 76000, 130000, 190000 and 214000 timesteps. The droplet splits evenly as the microchannel geometry is symmetrical.

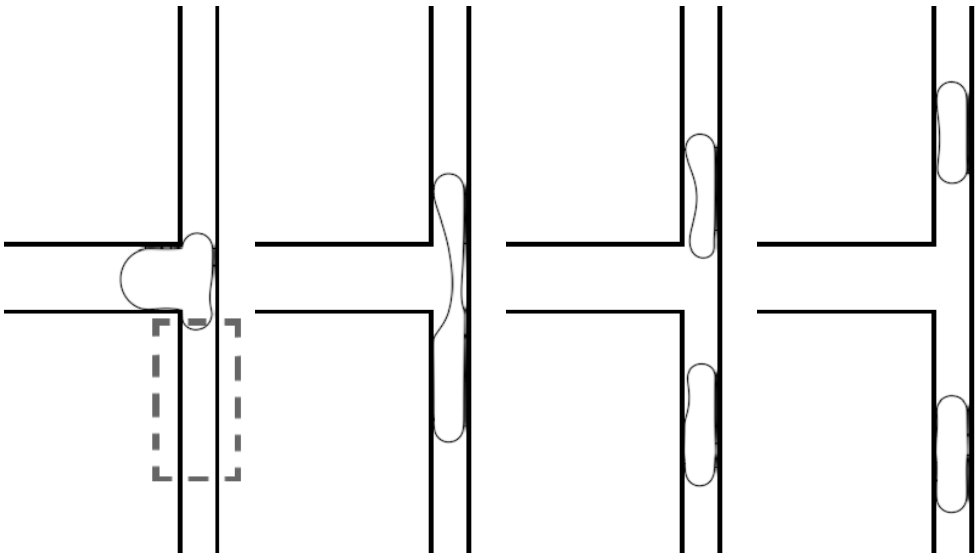

Figure 5: Droplet splitting at the T-junction with time taken at 76000, 130000, 156000 and 182000 timesteps when the heater, indicated by the area within the dashed lines, is switched on. We set the heater temperature $T=10$ and $\sigma_T=-0.001$. The temperature difference at the heater on the lower microchannel branch results in the lower daughter droplet being larger than the upper daughter droplet.

cous force from the carrier fluid overcomes the capillary force of the droplet, splitting the droplet into two equal parts due to the microchannel symmetry, which is shown in Fig. 4. When the heater is on, mimicked by setting the wall temperature to be 10 in the heated section, the temperature difference creates an interfacial tension gradient at the fluid-fluid interface near the lower microchannel branch. This pulls the droplet towards the lower microchannel branch and causes the droplet to split unevenly, with the lower daughter droplet being larger in size than the upper daughter droplet as shown in Fig. 5.

In the experimental study by Yap et al. [45] which uses a similar setup to our simulations, when the heater was switched off the incoming droplet was found to split evenly; when the heater was switched on, the droplets were found to split unevenly and in the extreme case (i.e. when the thermal gradient is large enough), the droplet would not split and would only enter the lower microchannel branch. Our simulation results show similar behaviour, suggesting an important role of thermocapillary force in droplet split.

4 Conclusion

In this study, our lattice Boltzmann model, which can describe thermocapillary force, is used to study microdroplet flows under thermal gradients. We demonstrate that the thermocapillary effects can be exploited to manipulate droplet dynamical behaviour and provide a novel approach for droplet synchronisation, sorting and splitting.

References

[1] R. B. Fair, Digital microfluidics: is a true lab-on-a-chip possible?, Microfluid. Nanofluidics, 3(2007), 245-281.

[2] H. Song, D. L. Chen and R. F. Ismagilov, Reactions in droplets in microfluidic channels, Angew. Chem., Int. Ed., 45(2006), 7336-7356.

[3] J. J. Agresti, E. Antipov, A. R. Abate, K. Ahn, A. C. Rowat, J.-C. Baret, M. Marquez, A. M. Klibanov, A. D. Griffiths and D. A. Weitz, Ultrahigh-throughput screening in drop-based microfluidics for directed evolution, PNAS, 107(2010), 4004-4009.

[4] M. Prakash and N. Gershenfeld, Microfluidic bubble logic, Science, 315(2007) 832-835.

[5] L. F. Cheow, L. Yobas and D.-L. Kwong, Digital microfluidics: Droplet based logic gates, Appl. Phys. Lett., 90(2007), 054107.

[6] K. Choi, A. H.C. Ng, R. Fobel and A. R. Wheeler, Digital microfluidics, Annu. Rev. Anal. Chem., 5(2012), 413-440.

[7] Z. J. Jiao, X. Y. Huang and N.-T. Nguyen, Manipulation of a droplet in a planar channel by periodic thermocapillary actuation, J. Micromech. Microeng. 18(2008), 045027.

[8] M.-C. Liu, J.-G. Wu, M.-F. Tsai, W.-S. Yu, P.-C. Lin, I-C. Chiu, H.-A. Chin, I-C. Cheng, Y.-C. Tung and J.-Z. Chen, Two dimensional thermoelectric platforms for thermocapillary droplet actuation, RSC Adv., 2(2012), 1639-1642.

[9] M. L. Cordero, D. R. Burnham, C. N. Baroud and D. McGloin, Thermocapillary manipulation of droplets using holographic beam shaping: microfluidic pin ball, Appl. Phys. Lett., 93(2008), 034107.

[10] C. Baroud, J.-P. Delville, F. Gallaire and R. Wunenburger, Thermocapillary valve for droplet production and sorting, Phys. Rev. E, 75(2007), 046302.

[11] C. Baroud, M. R. de Saint Vincent and J.-P. Delville, An optical toolbox for total control of droplet microfluidics, Lab Chip, 7(2007), 1029-1033.

[12] M. R. de Saint Vincent, R. Wunenburger and J.-P. Delville, Laser switching and sorting for high speed digital microfluidics, Appl. Phys. Lett., 92(2008), 154105.

[13] C. Hirt and B. Nichols, Volume of fluid (VOF) method for the dynamics of free boundaries, J. Comput. Phys. 39(1981), 201-225.

[14] S. Osher and J. A. Sethian, Fronts propagating with curvature-dependent speed: Algorithms based on Hamilton-Jacobi formulations, J. Comput. Phys., 79(1988), 12-49.

[15] W. Shyy, R. W. Smith, H. S. Udaykumar and M. M. Rao, Computational Fluid Dynamics with Moving Boundaries, Taylor & Francis, Washington, DC (1996).

[16] H.-Y. Chen, D. Jasñow and J. Vinals, Interface and contact line motion in a two phase fluid under shear flow, Phys. Rev. Lett., 85(2000), 1686-1689.

[17] S. Chen and G. D. Doolen, Lattice Boltzmann method for fluid flows, Annu. Rev. Fluid Mech., 30(1998), 329-364.

[18] A. K. Gunstensen, D. H. Rothman, S. Zaleski and G. Zanetti, Lattice Boltzmann model of immiscible fluids, Phys. Rev. A, 43(1991), 4320-4327.

[19] M. R. Swift, W. R. Osborn and J. M. Yeomans, Lattice Boltzmann simulation of nonideal fluids, Phys. Rev. Lett., 75(1995), 830-833.

[20] M. R. Swift, E. Orlandini, W. R. Osborn and J. M. Yeomans, Lattice Boltzmann simulations of liquid-gas and binary fluid systems, Phys. Rev. E, 54(1996), 5041-5052.

[21] X. Shan and H. Chen, Lattice Boltzmann model for simulating flows with multiple phases and components, Phys. Rev. E, 47(1993), 1815-1819.

[22] X. He, S. Chen and R. Zhang, A lattice Boltzmann scheme for incompressible multiphase

flow and its application in simulation of Rayleigh-Taylor instability, J. Comput. Phys., 152(1999), 642-663.
[23] J. Zhang, Lattice Boltzmann method for microfluidics: models and applications, Microfluid. Nanofluidics, 10(2011), 1-28.
[24] H. Liu, Y. Zhang and A. J. Valocchi, Modeling and simulation of thermocapillary flows using lattice Boltzmann method, J. Comput. Phys., 231(2012), 4433-4453.
[25] M. Latva-Kokko and D. H. Rothman, Diffusion properties of gradient-based lattice Boltzmann models of immiscible fluids, Phys. Rev. E, 71(2005), 056702.
[26] H. Liu, A. J. Valocchi, Y. Zhang and Q. Kang, A phase-field-based lattice-Boltzmann finite-difference model for simulating thermocapillary flows, Phys. Rev. E, 87(2013), 013010.
[27] H. Liu, A. J. Valocchi, Y. Zhang and Q. Kang, Lattice Boltzmann phase-field modeling of thermocapillary flows in a confined microchannel, J. Comput. Phys., 256(2014), 334-356.
[28] G. R. McNamara and G. Zanetti, Use of the Boltzmann equation to simulate lattice-gas automata, Phys. Rev. Lett., 61(1988), 2332-2335.
[29] F. J. Higuera and J. Jiménez, Boltzmann approach to lattice gas simulations, Europhys. Lett., 9(1989), 663-668.
[30] P. L. Bhatnagar, E. P. Gross and M. Krook, A model for collision processes in gases. I. Small amplitude processes in charged and neutral one-component systems, Phys. Rev., 94(1954), 511-525.
[31] Y. H. Qian, D. d'Humieres and P. Lallemand, Lattice BGK models for Navier-Stokes equation, Europhys. Lett., 17(1997), 479-484.
[32] J. M. V. A. Koelman, A simple lattice Boltzmann scheme for Navier-Stokes fluid flow, Europhys. Lett., 15(1991), 603-607.
[33] J. U. Brackbill, D. B. Kothe and C. Zemach, A continuum method for modeling surface tension, J. Comp. Phys., 100(1992), 335-354.
[34] Z. Guo, C. Zheng and B. Shi, Discrete lattice effects on the forcing term in the lattice Boltzmann method, Phys. Rev. E, 65(2002), 046308.
[35] I. Ginzburg and P. M. Adler, Boundary flow condition analysis for the three-dimensional lattice Boltzmann model, J. Phys. II France, 4(1994), 191-214.
[36] S. V. Lishchuk, C. M. Care and I. Halliday, Lattice Boltzmann algorithm for surface tension with greatly reduced microcurrents, Phys. Rev. E, 67(2003), 036701.
[37] M. Sbragaglia, R. Benzi, L. Biferale, S. Succi, K. Sugiyama and F. Toschi, Generalized lattice Boltzmann method with multirange pseudopotential, Phys. Rev. E, 75(2007), 026702.
[38] I. Halliday, A. P. Hollis and C. M. Care, Lattice Boltzmann algorithm for continuum multicomponent flow, Phys. Rev. E, 76(2007), 026708.
[39] H. Liu and Y. Zhang, Droplet formation in microfluidic cross-junctions, Phys. Fluids, 23 (2011), 082101.
[40] C. K. Aidun and J. R. Clausen, Lattice-Boltzmann method for complex flows, Annu. Rev. Fluid Mech. 42(2010), 439-472
[41] Q. Zou and X. He, On pressure and velocity boundary conditions for the lattice Boltzmann BGK model, Phys. Fluids, 9(1997), 1591-1598.
[42] C.-H. Liu, K.-H Lin, H.-C. Mai and C.-A. Lin, Thermal boundary conditions for thermal lattice Boltzmann simulations, Comput. Math. Appl., 59(2010), 2178-2193.
[43] B. Ahn, K. Lee, R. Panchapakesan and K. W. Oh, Parallel synchronization of two trains of droplets using a railroad-like channel network, Lab Chip, 11(2011), 3956-3962
[44] J. Maddala, B. Srinivasan, S. S. Bithi, S. A. Vananalli and R. Rengaswamy, Design of a model-based feedback controller for active sorting and synchronising of droplets in a microfluidic

loop, AICHE Journal, 58(2012), 2120-2130.
[45] Y. F. Yap, S. H. Tan, N. T. Nguyen, S. M. Sohel Murshed, T. N. Wong and L. Yobas, Thermally mediated control of liquid microdroplets at a bifurcation, J. Phys. D: Appl. Phys., 42(2009) 065503.
[46] J. Meng, Y. Zhang, N. G. Hadjiconstantinou, G. A. Radtke and X. Shan, Lattice ellipsoidal statistical BGK model for thermal non-equilibrium flows, J. Fluid Mech., 718(2013), 347-370